ADVANCED FUNCTIONAL MATERIALS
www.afm-journal.de

Aggregation-Enhanced Photoluminescence and Photoacoustics of Atomically Precise Gold Nanoclusters in Lipid Nanodiscs (NANO^2)

*Armin Tahmasbi Rad, Yue Bao, Hyun-Sook Jang, Yan Xia, Hari Sharma, Elena E. Dormidontova, Jing Zhao, Jaspreet Arora, Vijay T. John, Ben Zhong Tang, Tiziano Dainese, Ali Hariri, Jesse V. Jokerst, Flavio Maran, and Mu-Ping Nieh**

The authors designed a structurally stable nano-in-nano (NANO^2) system highly capable of bioimaging via an aggregation-enhanced NIR excited emission and photoacoustic response achieved based on atomically precise gold nanoclusters protected by linear thiolated ligands [$Au_{25}(SC_nH_{2n+1})_{18}$, $n = 4$–16] encapsulated in discoidal phospholipid bicelles through a one-pot synthesis. The detailed morphological characterization of NANO^2 is conducted using cryogenic transmission electron microscopy, small/wide angle X-ray scattering with the support of molecular dynamics simulations, providing information on the location of Au nanoclusters in NANO^2. The photoluminescence observed for NANO^2 is 20–60 times more intense than that of the free Au nanoclusters, with both excitation and emission wavelengths in the near-infrared range, and the photoacoustic signal is more than tripled. The authors attribute this newly discovered aggregation-enhanced photoluminescence and photoacoustic signals to the restriction of intramolecular motion of the clusters' ligands. With the advantages of biocompatibility and high cellular uptake, NANO^2 is potentially applicable for both in vitro and in vivo imaging, as the authors demonstrate with NIR excited emission from in vitro A549 human lung and the KB human cervical cancer cells.

1. Introduction

Development of biocompatible functional nanomaterials for in vivo applications remains a substantial challenge. These materials have to perform multiple functions and satisfy numerous requirements, starting from simplicity and reproducibility of preparation to robust imaging and solid performance in cells. Here, we report the development and properties of a novel nano-in-nano (NANO^2) platform through trapping thiolate-protected gold nanoclusters (AuNCs), such as $Au_{25}(SC_{16}H_{33})_{18}$ (Au-C16),[1] in a well-defined lipid-based nanodisc.[2] NANO^2 spontaneously forms via hydrophobic interactions between the lipid tails and the linear thiolated ligands, which protect the gold core, and is a potential candidate for theranostic nanocarrier due to

Dr. A. Tahmasbi Rad, Y. Bao, Prof. M.-P. Nieh
Department of Biomedical Engineering
University of Connecticut
Storrs, CT 06269, USA
E-mail: Mu-Ping.Nieh@uconn.edu
Dr. A. Tahmasbi Rad, Dr. H.-S. Jang, Prof. E. E. Dormidontova, Prof. M.-P. Nieh
Polymer Program
Institute of Materials Science
University of Connecticut
Storrs, CT 06269, USA
Dr. H.-S. Jang
Center for Soft and Living Matter
Institute for Basic Science (IBS)
Ulsan 44919, Republic of Korea
Dr. Y. Xia, Prof. M.-P. Nieh
Department of Chemical and Biomolecular Engineering
University of Connecticut
Storrs, CT 06269, USA
Dr. H. Sharma, Prof. E. E. Dormidontova
Department of Physics
University of Connecticut
Storrs, CT 06269, USA
Prof. J. Zhao, Prof. F. Maran
Department of Chemistry
University of Connecticut
Storrs, CT 06269, USA
Dr. J. Arora, Prof. V. T. John
Department of Chemical and Biomolecular Engineering
Tulane University
New Orleans, LA 70118, USA
Prof. B. Z. Tang
Department of Chemistry
the Hong Kong University of Science and Technology
Hong Kong, P. R. China
Dr. T. Dainese, Prof. F. Maran
Department of Chemistry
University of Padova
Padova 35131, Italy
A. Hariri, Prof. J. V. Jokerst
Department of NanoEngineering
University of California San Diego
La Jolla, CA 92093, USA
The ORCID identification number(s) for the author(s) of this article can be found under https://doi.org/10.1002/adfm.202009750.

DOI: 10.1002/adfm.202009750

significant aggregation-enhanced emission (AEE) and photoacoustics (AEP) together with the previously reported properties of high cellular uptake and efficacious treatment on cancer cells.[2]

The study of the properties and applications of atomically precise AuNCs, which consist of well-defined numbers of Au atoms (forming metal core of less than 2 nm) and capping ligands is an ever-growing area of current research.[3] Due to quantum-confinement effects, these nanoclusters have discrete electron-energy states that cause the emergence of specific properties and even molecular behavior, such as a HOMO-LUMO gap,[3f] distinct redox behavior,[3d] magnetism,[3e] and photoluminescence (PL).[3a,b,4] In contrast to larger Au nanoparticles, which show a strong localized surface plasmon resonance (instead of emission),[4] some AuNCs exhibit photoluminescence in solution depending on the number of Au atoms,[4a] the protecting ligands (type and length),[3b,4c,e,5] the charge density of the Au core,[4c,e,5,6] the ratio between the surface and core Au atoms, as well as additional factors.[4f,6a] To utilize the unique optical properties of AuNCs for in vivo applications, AuNCs should be loaded at high density in biocompatible carriers that are capable of incorporating targeting groups to achieve a high accumulation of these NC systems at desired sites. In the past, we examined several biocompatible lipid systems potentially applicable for theranostic delivery.[2,7] One of them is a discoidal aggregate (bicelle) that consists of a phospholipid mixture of biocompatible dipalmitoyl phosphatidylcholine (DPPC, di-C_{16}PC) and dihexanoyl phosphatidylcholine (DHPC, di-C_6PC), lightly doped with dipalmitoyl phosphatidylgylcerol (DPPG, di-C_{16}PG) to enhance the structural stability.[8] Such nanodiscs generally exhibit a uniform radius and bilayer thickness of 10–15 and 5 nm, respectively. Previous studies demonstrated 5–10 times enhancement in cellular uptake of bicelles in comparison with that of the vesicles made of an identical chemical composition,[2a,8a,b] which also indicated the surface of bicelles and vesicles can be modified by targeting ligands to target cancer cells specifically.

Here we report the formation and properties of NANO^2 with AuNCs entrapped in bicellar nanodiscs. These aggregates were characterized by cryogenic transmission electron microscopy (cryo-TEM) and small angle X-ray scattering (SAXS), and also studied by molecular dynamics (MD) simulations. We found that NANO^2 can be excited and emit at wavelengths in the near-infrared (NIR) region, which have deeper penetration through biological tissues. Moreover, the PL is greatly enhanced compared with that of the dispersed AuNCs, suggesting strong AEE. NANO^2 also exhibits a strong photoacoustic signal, significantly higher than that of a common photoacoustic agent (e.g., indocyanine green), thereby providing another potential application for high-sensitivity and high-resolution bioimaging. The easy one-pot synthesis, well-controlled nanostructure, good structural stability, high cellular uptake, and high AEE/AEP response make NANO^2 an excellent candidate for in vitro and in vivo contrast agents for general biomedical applications, as indeed supported by our preliminary data on the NIR excited emission from in vitro A549 human lung and the KB human cervical cancer cells.

2. Results and Discussion

2.1. AuNCs Properties

Hydrophobic $Au_{25}(SC_{16}H_{33})_{18}$ (Au-C16) is fully soluble in organic solvents, forming yellowish-brown solutions with a molar extinction coefficient of 5.5×10^4 M^{-1} cm^{-1} at 400 nm.[1] SAXS data of Au-C16 clusters in benzene yield an average radius of gyration of Au core, $\langle R^2_{G,core}\rangle^{\frac{1}{2}}$ of 0.37 nm through Guinier analysis (Figure S1(a), Supporting Information). The estimated core radius is 0.48 nm based on a spherical approximation, in excellent agreement with the value of 0.49 nm observed in the crystallographic structure of Au_{25} clusters.[9] The Stokes radius of Au-C16, which includes the monolayer effective thickness, is 1.67 nm.[9b,10]

2.2. AuNCs Encapsulation: Formation of NANO^2

Two NANO^2 samples with the individual Au-C16:lipid ratios of 1:500 and 1:67 were made and purified after centrifugation at 5000 rpm for 10 min to remove the unencapsulated Au-C16. UV–vis absorption was then conducted on the supernatant, which was redispersed in chloroform after being dried, and then compared against the calibration curve to identify the quantity of the encapsulated Au-C16. The observed encapsulation rate, which is defined as $ER = \frac{\text{Encapsulated AuNC Mass}}{\text{Initial AuNC Mass}}$, was 67.3% and 83.0% for the 1:500 and 1:67 samples, respectively. To the best of our knowledge, these values are higher than the highest reported value for other lipid nanocarriers in the literature (≈41%).[11] It is noteworthy that the sample with a lower AuNC:lipid ratio does not necessarily yield a higher ER, suggesting that some inhomogeneity in the AuNC aggregates might exist during the solvent-drying process, and therefore, that such aggregates could not be accommodated in the bicelles with a thickness of ≈5 nm. **Figure 1**a,b show the cryo-TEM images of NANO^2 (AuNC:lipid = 1:67) and suggest that the discoidal morphology was not affected by the entrapment of Au-C16. Furthermore, the hydrodynamic radius, R_H of NANO^2 was measured by dynamic light scattering (DLS). As shown in Figure S1 (b), Supporting Information, the R_H of pristine bicelles and NANO^2 (AuNC:lipid ≤ 1:67) are in the range of 10–12 and 15–20 nm, respectively, with a narrow distribution. However, NANO^2 with AuNC:lipid = 1:33 shows significant amount of large aggregates with a secondary population at ≈300 nm.

2.3. Optical Properties of $Au_{25}(SC_nH_{2n+1})_{18}$ and NANO^2

Au-C16 in chloroform shows minimal PL (NIR laser excitation at λ_{ex} = 785 nm) (**Figure 2**a) consistent with the results reported for other Au_{25} systems.[5,12] It has been shown that PL in AuNCs may depend on several factors, such as the size of the Au core,[4a] surface ligands,[4c,e,5] charge density of the Au core,[4c,e,5,6,13] and restriction of intramolecular motion (RIM) of the AuNC.[14] Figure 2a shows that the AuNC aggregates in NANO^2 exhibit a significant increase in PL peaking at a NIR

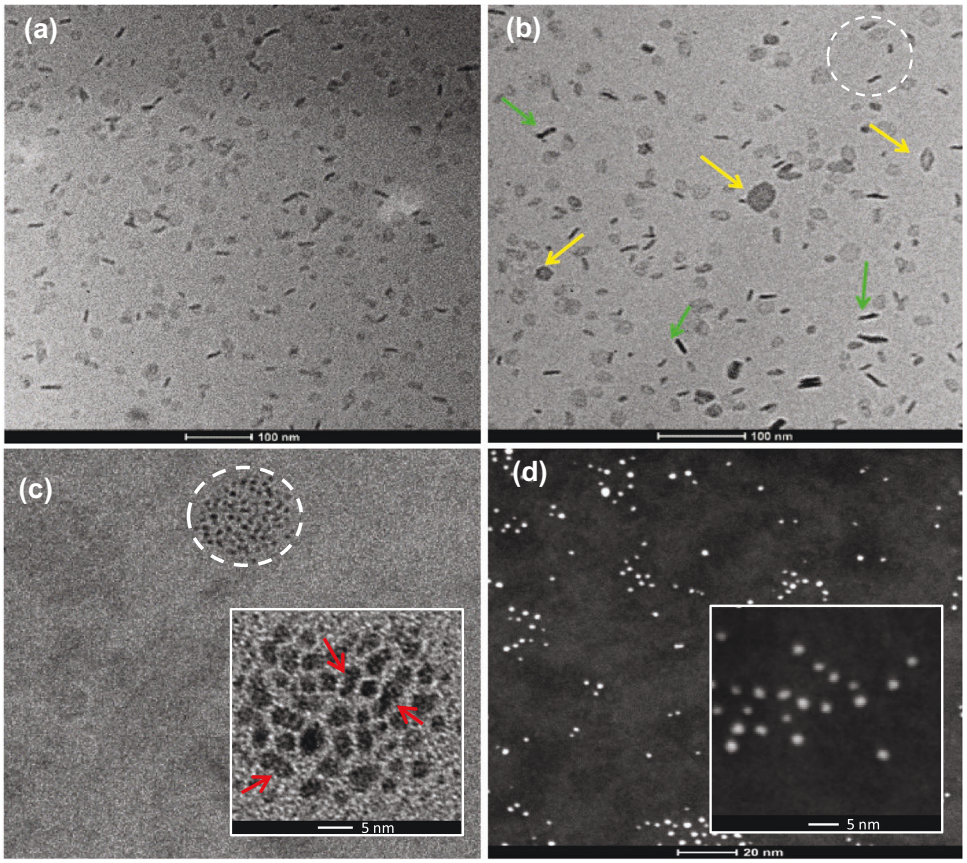

Figure 1. The cryo-TEM micrographs of a) pristine bicelles, and b) NANO^2-Au-C16 (Au-C16:lipid = 1:67). The arrows show the Au-C16 filled nanodiscs. The planar and rim views are indicated by yellow and green arrows, respectively. c) High magnification images of NANO^2-Au-C16 (Au-C16:lipid = 1:67) evidencing the presence of Au-C16 aggregates inside the bicelles. Two types of Au—Au distances observed: a center-to-center distance of 1–2 nm (red arrows) and the other of 4–5 nm range. d) High magnification of dried aggregated AuNCs after dissolving in chloroform. Some aggregated clusters can be observed in this case as well.

wavelength of ca. 870 nm. This AEE is conceivably caused by a RIM effect, as the chemistry of AuNCs is identical before and after entrapment. The RIM mechanism was mainly proposed for some organic fluorogens, most of which contained intramolecular "rotors"[15] leading to AEE because the pathway of energetic dissipation was altered from a nonradiative to emissive mechanism due to RIM.[14] Our observation suggests that such RIM-induced AEE may also take place in the entrapped AuNCs. A very recent observation of AEE in the NIR for AuNCs capped with glutathione and entrapped in chitosan nanogels[16] provides further support to the hypothesis of a RIM mechanism.[16] We found a similar PL in dried AuNC samples, albeit with a slight blue shift (Figure 2a; Figure S2, Supporting Information) compared to NANO^2, confirming that the observed NIR photoluminescence is induced by the aggregation of AuNCs (Figure 1c). It is also worth mentioning that this AEE can be observed also for Au_{25} clusters protected by shorter thiolated ligands (Figure S3, Supporting Information). Figure 2b shows that the PL significantly diminishes when NANO^2 is dissociated in a mixture of chloroform and dimethylformamide (at the same AuNC concentration). This observation indicates that AuNC aggregation is indeed the key to the observed AEE.

The PL of NANO^2 is also observed for the Au-C16:lipid = 1:500 sample. In fact, the AEE normalized for the actual concentration of encapsulated AuNCs, increases when the Au-C16/lipid ratio decreases, as shown in Figure 2d. This effect can be attributed to several causes, such as a nonlinear AEE response with AuNC concentration, possible self-quenching of the AEE, unevenly distributed AuNCs in NANO^2, and strong reabsorption of the AEE wavelength. Another noteworthy observation is that the UV–vis absorption spectra of NANO^2 (Figures S4–S6, Supporting Information) seem to exhibit higher absorption than those of the corresponding free AuNC solutions (in benzene)[1] at the same AuNC concentration. The increase of adsorption likely provides some insights to the AEE, requiring more investigation to fully understand the reason.

2.4. Nanostructural Characterization of AuNCs in NANO^2

To assess the representativity of the cryo-TEM images shown in Figure 1a–d and to provide insights into the structure-property relationship, nanostructural characterization was performed with SAXS on the pristine bicelle and NANO^2 with Au-C16:lipid molar ratios of 1:500 and 1:67 (**Figure 3**a). A core-shell discoidal (CSD) model (Section 5, Supporting Information) with seven fitting

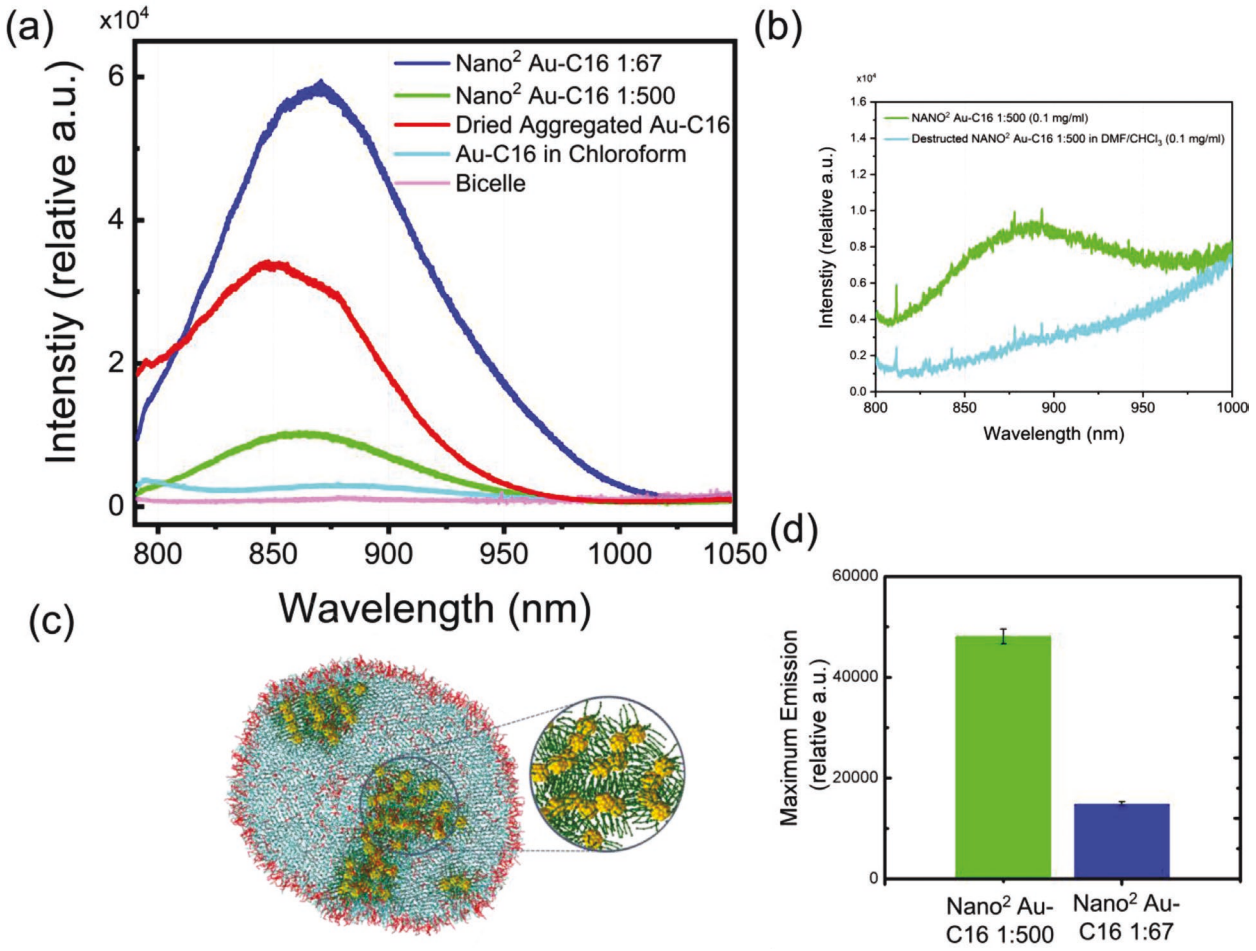

Figure 2. Photoluminescence spectra of a) NANO^2-Au-C16 at an initial Au-C16:lipid ratio of 1:67 and 1:500 compared with the Au-C16 in chloroform solution at a similar concentration to the 1:67 sample. The experiment was performed on a Raman microscopy excited by a laser at 785 nm. The spectra of Au-C16 in chloroform at the same Au concentration and pristine bicelles are also presented, indicating no-photoluminescence. b) Photoluminescence of 1 ml solution of NANO^2-Au-C16 (0.1 mg ml^{-1} with an AuNC:lipid = 1:500) obtained upon dilution of a 0.2 mg ml^{-1} NANO^2-Au-C16 sample solution with water (green) or with a 1:1 (volume ratio) solution of DMF:$CHCl_3$ (cyan). In the latter sample, the discoidal NANO^2 structure is presumably destroyed. The excitation wavelength was 785 nm. c) MD simulation snapshot of NANO^2-Au-C16 with encapsulated Au-C16 clusters (shown in yellow with green tethers). DPPC is shown in cyan, DHPC in red. d) Normalized peak intensities by the entrapped quantity of AuNCs for the NANO^2-Au-C16 (Table S1, Supporting Information) as a function of the initial Au-C16:lipid ratio.

parameters, core radius (R_{core}), core axial thickness (t_{core}), axial shell thickness (t_{axial}), rim shell thickness (t_{rim}), electron scattering length densities of core (ρ_{core}), axial shell (ρ_{axial}), and rim shell (ρ_{rim}), respectively, has been used to describe the scattering pattern of the bicelle structure.[8a,d,17] The best fits (Figure S7, Supporting Information) agree with the SAXS data well, resulting in the best fitting parameters of pristine bicelle and NANO^2 (at Au-C16:lipid = 1:500) as listed in **Table 1**. The total bilayer thickness (t_{core} + $2t_{axial}$, ≈5.5–5.8 nm) is practically invariant, the drastic increase of t_{rim} (from 1.4 nm to 6.0 nm) and increased ρ_{rim} (from 9.72×10^{-6} to 10.1×10^{-6} Å^{-2}) in NANO^2 compared to the pristine bicelles suggest that at the low Au-C16:lipid ratio of 1:500 most of the entrapped Au-C16 is preferably localized near the disc rim. This can be explained by the fact that disc rim, which is mainly composed of short-chain DHPC, has a large spontaneous curvature and is more fluidic,[18] thereby making it possible to accommodate higher-curvature objects like AuNCs (Figure 3c), consistent with previous MD simulations,[19] and further enhancing ER. Note that the best fits to the SAXS data of all NANO^2, whose AuNCs were conjugated with different ligand lengths (from C4 to C16), revealed discoidal morphology at the same AuNC-to-lipid ratio of 1:500 (Figure S7, Supporting Information).

For the higher Au-C16:lipid ratio of 1: 67 NANO^2, the SAXS pattern (Figure 3b) exhibits further sharp diffraction peaks, and therefore, cannot be accommodated by the same CSD model. High-order diffraction peaks in the wide angle X-ray scattering (WAXS) regime indicate a well-ordered structure. Identical peak positions were also found in dried Au-C16 in the absence of lipids, suggesting that they originate from the inter-cluster core-to-core distance (d_{cc}) due to aggregation. The first-order Bragg's reflection, q_{p1}, corresponds to d_{cc} according to the expression, $d_{cc} \approx \frac{2\pi}{q_{p1}}$. We have found that d_{cc} decreases when the ligand length decreases, and this suggests that a good portion of AuNCs (in both dried and encapsulated states) are spaced by the ligands between the clusters without their cores

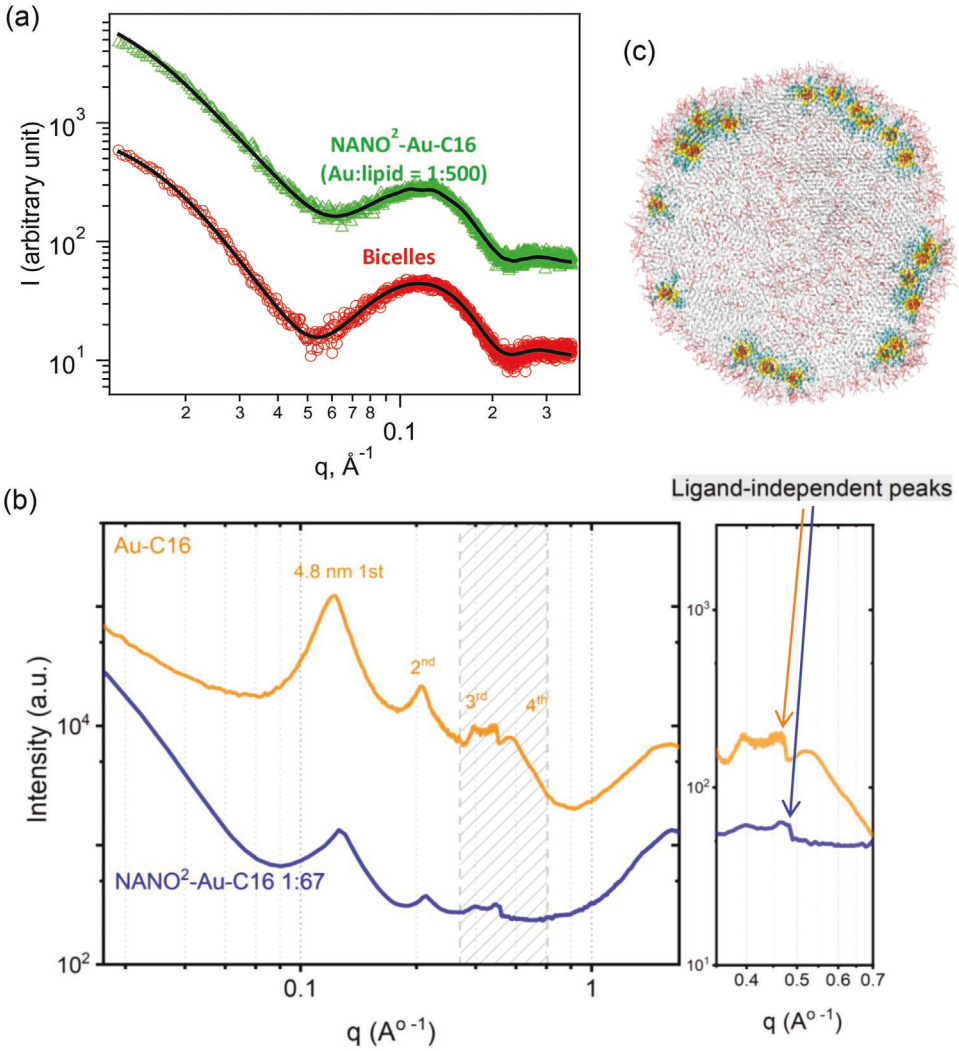

Figure 3. a) SAXS data of pristine bicelles (red circles) and NANO^2-Au-C16 with Au-C16:lipid ratio of 1:500 (green triangles) at 10 °C. The solid curves are the best fits to the SAXS data with the best fitting parameters listed in Table 1. b) SAXS/WAXS data of dry Au-C16 (orange) and NANO^2-Au-C16 with Au-C16:lipid ratio of 1:67 (blue) at 10 °C (blue) with a blow-up shaded region on the right panel. c) MD simulation snapshot shows Au-C16 encapsulated into the rim of NANO^2 consistent with the SAXS interpretation in (a).

touching each other (Figure S8, Supporting Information). The fact that the d_{cc} value obtained from NANO^2 is nearly the same as in the dry state implies that the majority of AuNC aggregates in NANO^2 do not involve lipids sandwiched between them, otherwise d_{cc} would have increased. Another peak, which is independent of ligand lengths (highlighted in the blow-up shaded regions of Figure 3b; Figure S8, Supporting Information), was found at 0.48 Å^{-1}. This corresponds to 1.31 nm and is thus consistent with the closest core-to-core (center-to-center) distances of 1.26–1.30 nm measured by single-crystal X-ray crystallography in the polymers made of Au_{25} nanoclusters.[9b,20] Presently, it is not conclusive if the AEE is related to either of the configurations or independent of AuNC arrangement.

Table 1. The best fitting parameters for SAXS data of bicelle and NANO^2-Au-C16 (Au-C16:lipid = 1:500) at room *T* using CSD.

	bicelle	NANO^2
R_{core}(nm)	10.5(±0.8)	>30
t_{core}(nm)	2.8(±0.1)	2.7(±0.4)
t_{axial}(nm)	1.5(±0.5)	1.4(±0.3)
t_{rim}(nm)	1.4(±0.4)	6.0(±0.6)
	Electron density (×10^{-6}Å^{-2})	
Core	8.69(±0.08)	8.61(±0.03)
Shell (axial)	10.6(±0.13)	10.7(±0.03)
Shell (rim)	9.72(±0.06)	10.1(±0.05)

2.5. Molecular Dynamics Simulations

Coarse-grained MD simulations were performed on the NANO^2-Au-C16 to investigate the arrangement of Au-C16 inside the bicelles. A snapshot of the Au-C16 clustering in the bicelles, as exemplified in Figure 3c, suggests that the discoidal morphology is indeed not significantly disturbed

by the presence of encapsulated Au-C16 clusters, in agreement with the TEM micrographs and SAXS data. Accordingly, the radial distribution functions for Au-C16 show a strong peak at a core-to-core separation distance of about 1.25 nm (Figure S9, Supporting Information), consistent with the S/WAXS peaks, and additional weaker peaks at larger ligand-dependent distances corresponding to the aforementioned Bragg's reflections with high-order harmonics in the S/WAXS data (Figure 3b). The location of AuNCs depends on the experimental conditions for NANO^2 preparation. Figure 3c shows a snapshot of MD simulations if the AuNCs are initially placed either nearby the rim or in the aqueous phase. The AuNCs would enter the disc and stay at the bicellar rim,[19] resulting in higher electron density at the discoidal rim of NANO^2 than that of the pristine bicelles consistent with the SAXS data of NANO^2 with low AuNC concentration. However, if the AuNCs mix with lipids to form NANO^2 (at higher AuNC concentrations), the AuNCs can be located anywhere in the bicelle as shown in Figure 2c, consistent with the cryo-TEM micrographs of some NANO^2 (Figure 1c). The MD simulation also indicated a strong influence of the ligand length of the encapsulated AuNCs on the local DPPC lipid order. AuNCs capped by ligands matching the lipid tail length (as in Au-C16) yield a higher DPPC lipid order than those capped by shorter ligands (Table S2 and Figure S10, Supporting Information), suggesting that this could be the factor determining the higher encapsulation efficiency observed for Au-C16.

2.6. Applications of NANO^2 for In Vitro Study

Potential applications of NANO^2 were examined by carrying out an in vitro study on the A549 human lung cancer and the KB human cervical cancer cells after incubation with NANO^2. For biomedical applications, one of the major advantages of nanodiscs is their low-toxicity and high cellular uptake,[2,21] demonstrating their significant potential to transport molecules across the cell membrane. The cytotoxicity of the NANO^2 and pristine bicelles were evaluated against both human KB cervical and human A549 lung cancer cells. Pristine bicelles did not demonstrate any significant cytotoxicity even at high concentrations. NANO^2 samples, on the other hand, have shown slight cytotoxicity above 0.170 mM (1.6 mg mL^{-1}) as shown in Figure S12, Supporting Information, which is 50-fold concentration of the sample in the optical measurements. Therefore, NANO^2 can be considered nontoxic for diagnostic purposes. **Figure 4**a,b,c,d show the accumulation of NANO^2 at specific organelles in the A549 human lung and KB human cancer cells, respectively. The aggregation of the AuNCs was found mainly in the endoplasmic reticulum (ER) and Golgi apparatus (GA) after 2 h of incubation in both cell types.

Most importantly, the AEE of NANO^2-Au-C16 (at Au-C16:lipid = 1:67) persisted after cellular uptake, as demonstrated in Figure 4h, where the photoluminescent spectra of KB cells alone, KB/bicelles, NANO^2-Au-C16, and KB/NANO^2-Au-C16 are compared. KB cells were treated with the same concentration of the samples for 4 h. After washing the cells thoroughly with DPBS, samples were studied for their photoluminescent emission at the same condition. Samples that do not contain NANO^2-Au-C16 show essentially no emission. The fact that both KB/NANO^2 samples exhibit even higher emission (by a factor of 3–5) than that of the NANO^2 samples alone, suggests that the AEE-active arrangement of entrapped AuNCs is preserved and even enhanced in the in vitro experiment. Similar trends were observed for A549 lung cells as shown in Figure S11, Supporting Information. Most intriguingly, several sharp spikes, whose locations are independent of the ligand length in the AuNCs, were observed, presumably corresponding to surface-enhanced Raman scattering (SERS) of biomolecules nearby the aggregating AuNCs found in both ER and GA (Figure 4b,d), where biomolecules are abundant. Although SERS spectra of cells are complicated, signature peaks at 647, 840, 1003, 1038, 1179, 1205, 1460, and 1600 cm^{-1} have been observed in the SERS spectra of cervical cancer cells.[22] It is noteworthy that both excitation and emission wavelengths (785 and 800–950 nm, respectively) are in the NIR region, which entails a higher capability to penetrate biological tissues, suggesting the potential of our NANO^2 system as a promising in vivo diagnostic platform.

The potential of photoacoustics has been reported to be applicable for high-sensitivity and high resolution in vivo bioimaging.[23] We have evaluated the photoacoustic properties of the NANO^2 by 3D scanning of tubes containing individual samples as described in the Supporting Information. Figure 4e shows the photoacoustic images of NANO^2-Au-C16 1:67, 1:500 samples, the free Au-C16 in chloroform at the corresponding Au-C16 concentrations, and the pristine bicelles when illuminated at 720 nm laser light, which yielded the maximal PA signals for NANO^2. A standard photoacoustic dye, indocyanine green (ICG) was also encapsulated in the bicelle platform in order to compare with the NANO^2. PA signals of the free ICG (in water) and ICG-bicelle samples at a fixed concentration of 115 μg mL^{-1} were measured. Furthermore, fresh blood and free ICG were imaged at their maximum PA intensity (800 nm) as control samples. Figure 4f shows the photoacoustic spectra of all the samples acquired from 680 nm to 970 nm. Both NANO^2-Au-C16 solutions exhibited higher photoacoustic intensity than their corresponding free Au-C16 samples in chloroform. Furthermore, a comparison of Vis–NIR absorbance spectra among the samples shown in Figure 4g indicates that the absorbance of all samples containing AuNC is relatively steady over the probing range of wavelength from 700 nm to 1000 nm, and that the entrapment of AuNC in NANO^2 leads to higher absorbance. Moreover, the fact that the absorbance of ICG-containing samples is higher than that of the NANO^2 even with the higher AuNC content (1:67) below 800 nm provides partial reasoning for distinctly better performance of NANO^2-Au-C16 (1:67) than ICG at wavelength lower than 800 nm. The photoacoustic intensity of each sample is averaged from five different locations of interest in Figure 4e and summarized in Figure 4i. NANO^2-Au-C16 of 1:67 ratio illustrates the photoacoustic intensity more than three times of that yielded by Au-C16 at the same concentration in its free form. The evidence suggests that RIM effectively enhances the photoacoustic intensity in addition to AEE for the entrapped Au-C16 in NANO^2, a similar phenomenon observed in some other photoacoustic agent molecules after being trapped within a carrier.[24]

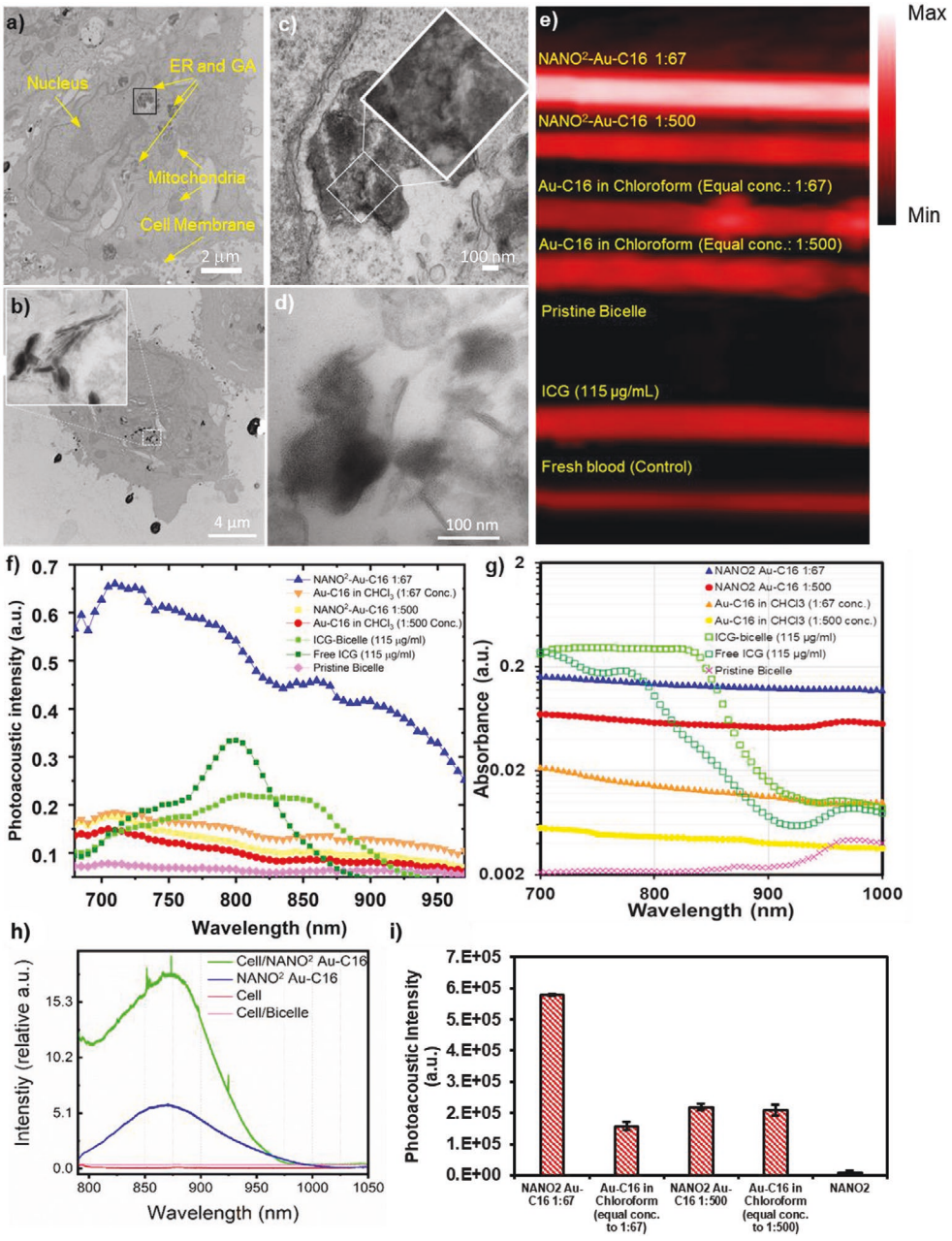

Figure 4. a,b) TEM images of the A549 human lung cancer cells after 2-h incubation with the NANO^2-Au-C16 at different magnifications. The majority of the endocytosed Au-C16 was observed at ER and GA. A slight population was also found in the mitochondria. c,d) TEM images of the KB cells, in which the aggregation of NANO^2-Au-C16 was also observed. The NANO^2 ultimately released AuNCs, causing noticeable aggregations in certain organelles (e.g., ER/GA). e) Photoacoustic images of the pristine bicelle, NANO^2-Au-C16 (1:500 and 1:67), free Au-C16 at corresponding Au-C16 concentrations, ICG solution (115 mg mL^{-1}), and fresh blood sample. f) Photoacoustic spectra of the samples in (e). g) The Vis–NIR absorption spectra of samples, at the NIR region. The intensities are plotted in logarithmic scale to demonstrate the significance of the samples. h) PL spectra of KB cells, KB/bicelles, KB/NANO^2, and NANO^2 alone as excited by 785 nm laser. All the samples have the same lipid concentration and Au-C16:lipid ratio of 1:67 except for KB cell alone. The spike-like signals observed in KB/NANO^2 are possibly SERS. i) Quantification analysis on photoacoustic outcomes in (d), showing enhanced photoacoustic property in NANO^2.

3. Conclusion

We describe a uniform-sized, self-assembled discoidal NANO^2 platform (bicelle/AuNC) that shows important AEE and AEP signals. Whereas the same Au-C16 does not exhibit noticeable photoluminescence as dispersed in solution, enhanced photoluminescence and photoacoustic intensity are observed upon encapsulation in NANO^2, presumably due to the RIM imposed on the ligands of Au-C16. The high encapsulation rate (>80%) can be attributed to Au-C16 clustering in the interior of the

bicell or at the high-curvature rim formed by the more mobile short-chain lipids, allowing interaction with hydrophobic molecules or objects.[18a] The experimental outcome is consistent with the MD simulation, which predicts that, depending on the initial AuNC-to-lipid ratio, the entrapped Au-C16 nanoclusters or their aggregates can be located preferentially at the rim, with concomitant stabilization of the discs, or be randomly distributed inside the bicelles.

Other than a high encapsulation rate, multiple advantages of our novel NANO^2 system, such as high biocompatibility, one-pot synthesis (high scalability), well-controlled size (high uniformity), high structural stability, and high cellular uptake,[2,7,8b,25] make it an ideal candidate for in vitro and in vivo biomedical applications. We have found that the NANO^2-Au-C16 appeared to be more stable than pristine bicelles, whose lifetime is normally less than 6 months (Figure S13, Supporting Information). The AEP in the NIR regime (for both excitation and emission wavelengths) and enhanced photoacoustic property demonstrate their high potential for applications in bioimaging. Moreover, it appears that the NANO^2 may enhance the Raman signal of biomolecules at the vicinity of biomolecules, which could be used for sensing specific target biomolecules in the cytoplasm. It should be finally noted that chemical modification on the surface of NANO^2 is readily achievable by proper co-mixing of amphiphilic functional molecules with the lipids, thereby imparting NANO^2 useful targeting properties.

Supporting Information

Supporting Information is available from the Wiley Online Library or from the author.

Acknowledgements

M.-P.N., Y.B., A.T.R., Y.X., H.-S.J., H.S., and E.E.D. would like to acknowledge National Science Foundation (NSF) for the financial supports (CBET 1605971). T.D. and F.M. acknowledge AIRC (Project 12214: Innovative Tools for cancer risk assessment and early diagnosis – 5 per mille) for financial support. The SAXS instrument was partially funded through NSF-MRI (DMR 1228817).

Conflict of Interest

The authors declare no conflict of interest.

Author Contributions

M.-P.N. and A.T.R. conceived and designed the study. A.T.R. and Y.B. synthesized and characterized NANO^2 and performed the experiments and analyzed the data. T.D. synthesized and characterized the AuNCs. H.-S.J. and J.Z. contributed to interpretation of the optical results. Y.X., Y.B., and M.-P.N. performed and analyzed X-ray scattering data. H.S. and E.E.D. conducted the MD simulation studies. J.A. and V.T.J. performed cryo-TEM experiments. F.M. provided the AuNC and discussed over the properties of AuNCs with M.-P.N., A.T.R., and E.E.D. All the authors contributed to the writing of the manuscript.

Keywords

aggregation-enhanced emission, aggregation-enhanced photoacoustic, bicelles, bioimaging, cellular endocytosis, gold nanocluster

Received: November 13, 2020
Published online: December 13, 2020

[1] S. Antonello, G. Arrigoni, T. Dainese, M. De Nardi, G. Parisio, L. Perotti, A. René, A. Venzo, F. Maran, *ACS Nano* **2014**, *8*, 2788.
[2] a) W. Aresh, Y. Liu, J. Sine, D. Thayer, A. Puri, Y. Huang, Y. Wang, M.-P. Nieh, *J. Biomed. Nanotechnol.* **2016**, *12*, 1852; b) A. Tahmasbi Rad, C.-W. Chen, W. Aresh, Y. Xia, P.-S. Lai, M.-P. Nieh, *ACS Appl. Mater. Interfaces* **2019**, *11*, 10505.
[3] a) R. Jin, C. Zeng, M. Zhou, Y. Chen, *Chem. Rev.* **2016**, *116*, 10346; b) T. Tsukuda, H. Häkkinen, *Protected Metal Clusters: From Fundamentals to Applications*, Elsevier, Amsterdam / New York **2015**; c) I. Chakraborty, T. Pradeep, *Chem. Rev.* **2017**, *117*, 8208; d) S. Antonello, F. Maran, *Curr. Opin. Electrochem.* **2017**, *2*, 18; e) M. Agrachev, S. Antonello, T. Dainese, M. Ruzzi, A. Zoleo, E. Aprà, N. Govind, A. Fortunelli, L. Sementa, F. Maran, *ACS Omega* **2017**, *2*, 2607; f) R. Jin, *Nanoscale* **2015**, *7*, 1549; g) H. Yu, B. Rao, W. Jiang, S. Yang, M. Zhu, *Coordination Chemistry Reviews* **2019**, *378*, 595; h) Q. Li, M. Zhou, W. Y. So, J. Huang, M. Li, D. R. Kauffman, M. Cotlet, T. Higaki, L. A. Peteanu, Z. Shao, *J. Am. Chem. Soc.* **2019**, *141*, 5314.
[4] a) Y. Negishi, Y. Takasugi, S. Sato, H. Yao, K. Kimura, T. Tsukuda, *J. Am. Chem. Soc.* **2004**, *126*, 6518; b) G. Wang, T. Huang, R. W. Murray, L. Menard, R. G. Nuzzo, *J. Am. Chem. Soc.* **2005**, *127*, 812; c) G. Wang, R. Guo, G. Kalyuzhny, J.-P. Choi, R. W. Murray, *J. Phys. Chem. B* **2006**, *110*, 20282; d) P. K. Jain, W. Huang, M. A. El-Sayed, *Nano Lett.* **2007**, *7*, 2080; e) Z. Wu, R. Jin, *Nano Lett.* **2010**, *10*, 2568; f) Z. Luo, X. Yuan, Y. Yu, Q. Zhang, D. T. Leong, J. Y. Lee, J. Xie, *J. Am. Chem. Soc.* **2012**, *134*, 16662; g) J. Zhang, Y. Fu, C. V. Conroy, Z. Tang, G. Li, R. Y. Zhao, G. Wang, *J. Phys. Chem. C* **2012**, *116*, 26561.
[5] Z. Tang, T. Ahuja, S. Wang, G. Wang, *Nanoscale* **2012**, *4*, 4119.
[6] a) N. Goswami, Q. Yao, Z. Luo, J. Li, T. Chen, J. Xie, *J. Phys. Chem. Lett.* **2016**, *7*, 962; b) M. Gao, F. Yu, C. Lv, J. Choo, L. Chen, *Chem. Soc. Rev.* **2017**, *46*, 2237.
[7] A. T. Rad, S. Malik, L. Yang, T. K. Oberoi-Khanuja, M.-P. Nieh, R. Bahal, *Nanoscale* **2019**, *11*, 12517.
[8] a) Y. Liu, M. Li, Y. Yang, Y. Xia, M.-P. Nieh, *Biochim. Biophys. Acta, Biomembr.* **2014**, *1838*, 1871; b) Y. Liu, Y. Xia, A. T. Rad, W. Aresh, M.-P. Nieh, *Liposomes. Methods in Molecular Biology*, Vol. *1522*, Humana Press, New York, NY **2017**, 273; c) A. Hu, T.-H. Fan, J. Katsaras, Y. Xia, M. Li, M.-P. Nieh, *Soft Matter* **2014**, *10*, 5055; d) M.-P. Nieh, P. Dolinar, N. Kucerka, S. R. Kline, L. M. Debeer-Schmitt, K. C. Littrell, J. Katsaras, *Langmuir* **2011**, *27*, 14308.
[9] M. W. Heaven, A. Dass, P. S. White, K. M. Holt, R. W. Murray, *J. Am. Chem. Soc.* **2008**, *130*, 3754.
[10] a) M. Zhu, C. M. Aikens, F. J. Hollander, G. C. Schatz, R. Jin, *J. Am. Chem. Soc.* **2008**, *130*, 5883; b) S. Antonello, T. Dainese, M. De Nardi, L. Perotti, F. Maran, *ChemElectroChem* **2016**, *3*, 1237.
[11] a) H. F. Salem, S. M. Ahmed, M. M. Omar, *Drug Des., Dev. Ther.* **2016**, *10*, 277; b) L. Paasonen, T. Sipilä, A. Subrizi, P. Laurinmäki, S. J. Butcher, M. Rappolt, A. Yaghmur, A. Urtti, M. Yliperttula, *J. Controlled Release* **2010**, *147*, 136.
[12] a) S. Wang, X. Zhu, T. Cao, M. Zhu, *Nanoscale* **2014**, *6*, 5777; b) L. Shang, N. Azadfar, F. Stockmar, W. Send, V. Trouillet, M. Bruns, D. Gerthsen, G. U. Nienhaus, *Small* **2011**, *7*, 2614; c) Y. Negishi, T. Iwai, M. Ide, *Chem. Commun.* **2010**, *46*, 4713;

d) D. Lee, R. L. Donkers, G. Wang, A. S. Harper, R. W. Murray, *J. Am. Chem. Soc.* **2004**, *126*, 6193.
[13] S. Gwo, H.-Y. Chen, M.-H. Lin, L. Sun, X. Li, *Chem. Soc. Rev.* **2016**, *45*, 5672.
[14] a) B.-R. Gao, H.-Y. Wang, Y.-W. Hao, L.-M. Fu, H.-H. Fang, Y. Jiang, L. Wang, Q.-D. Chen, H. Xia, L.-Y. Pan, *J. Phys. Chem. B* **2010**, *114*, 128; b) Y. Chen, J. W. Lam, R. T. Kwok, B. Liu, B. Z. Tang, *Mater. Horiz.* **2019**, *6*, 428.
[15] a) F. Bu, R. Duan, Y. Xie, Y. Yi, Q. Peng, R. Hu, A. Qin, Z. Zhao, B. Z. Tang, *Angew. Chem., Int. Ed.* **2015**, *54*, 14492; b) Y. Huang, J. Mei, X. Ma, *Dyes Pigm.* **2019**, *165*, 499.
[16] H. Liu, G. Hong, Z. Luo, J. Chen, J. Chang, M. Gong, H. He, J. Yang, X. Yuan, L. Li, *Adv. Mater.* **2019**, *31*, 1901015.
[17] S. Mahabir, D. Small, M. Li, W. Wan, N. Kučerka, K. Littrell, J. Katsaras, M.-P. Nieh, *Biochim. Biophys. Acta, Biomembr.* **2013**, *1828*, 1025.
[18] a) Y. Xia, H.-S. Jang, Z. Shen, G. D. Bothun, Y. Li, M.-P. Nieh, *Langmuir* **2017**, *33*, 5745; b) Y. Xia, K. Charubin, D. Marquardt, F. A. Heberle, J. Katsaras, J. Tian, X. Cheng, Y. Liu, M.-P. Nieh, *Langmuir* **2016**, *32*, 9757; c) Y. Xia, M. Li, K. Charubin, Y. Liu, F. A. Heberle, J. Katsaras, B. Jing, Y. Zhu, M.-P. Nieh, *Langmuir* **2015**, *31*, 12920.
[19] H. Sharma, E. E. Dormidontova, *ACS Nano* **2017**, *11*, 3651.
[20] M. De Nardi, S. Antonello, D.-e. Jiang, F. Pan, K. Rissanen, M. Ruzzi, A. Venzo, A. Zoleo, F. Maran, *ACS Nano* **2014**, *8*, 8505.
[21] A. T. Rad, S. Malik, L. Yang, T. K. Oberoi-Khanuja, M.-P. Nieh, R. Bahal, *Nanoscale* **2019**, *11*, 12517.
[22] A. Kamińska, T. Szymborski, E. Witkowska, E. Kijeńska-Gawrońska, W. Świeszkowski, K. Niciński, J. Trzcińska-Danielewicz, A. Girstun, *Nanomaterials* **2019**, *9*, 366.
[23] a) P. K. Upputuri, M. Pramanik, *Wiley Interdiscip. Rev.: Nanomed. Nanobiotechnol.* **2020**, *12*, e1618; b) C. Moore, J. V. Jokerst, *Theranostics* **2019**, *9*, 1550.
[24] J. Kang, D. Kim, J. Wang, Y. Han, J. M. Zuidema, A. Hariri, J. H. Park, J. V. Jokerst, M. J. Sailor, *Adv. Mater.* **2018**, *30*, 1800512.
[25] E. Blanco, H. Shen, M. Ferrari, *Nat. Biotechnol.* **2015**, *33*, 941.